Slovenská technická univerzita v Bratislave
Stavebná fakulta

Ing. Michal Kollár

Autoreferát dizertačnej práce

Solving partial differential equations on surfaces with applications to geodetic data analysis

na získanie akademického titulu *philosophiae doctor (PhD.)*
v doktorandskom študijnom programe
9.1.9 Aplikovaná matematika

Bratislava 2018

Dizertačná práca bola vypracovaná v dennej forme doktorandského štúdia na Katedre matematiky a deskriptívnej geometrie SvF STU v Bratislave.

Predkladateľ: Ing. Michal Kollár
Katedra matematiky a deskriptívnej geometrie
SvF STU, Bratislava

Školiteľ: Prof. RNDr. Karol Mikula, DrSc.
Katedra matematiky a deskriptívnej geometrie
SvF STU, Bratislava

Oponenti: Prof. RNDr. Igor Bock, PhD.
Ústav informatiky a matematiky
FEI STU, Bratislava

Doc. Ing. Gabriel Okša, CSc.
Oddelenie informatiky Matematického ústavu SAV
SAV, Bratislava

Doc. RNDr. Angela Handlovičová, CSc.
Katedra matematiky a deskriptívnej geometrie
SvF STU, Bratislava

Autoreferát bol rozoslaný dňa ....

Obhajoba dizertačnej práce sa koná dňa .... o .... hod. na Katedre matematiky a deskriptívnej geometrie SvF STU v Bratislave, Radlinského 11.

prof. Ing. Stanislav Unčík, PhD.
dekan Stavebnej fakulty

Abstract

The thesis deals with filtering of geodetic data on closed surfaces by using the linear, nonlinear and geometrical diffusion equations. The linear diffusion filtering is given by the Laplace-Beltrami operator representing linear diffusion along the surface. For the nonlinear diffusion filtering, we use Perona-Malik type nonlinear diffusion equations with diffusion coefficient depending on surface gradient and introduce a new model where diffusion coefficient depends on surface Laplacian of solution. This allows adaptive filtering respecting edges and local extrema in the data. Adaptive filtering is also performed by using the nonlinear geometrical diffusion driven by mean curvature of contour lines of data. For numerical discretization of all mentioned models, we develop a surface finite-volume method to approximate the partial differential equations on the closed surface. The surfaces are approximated by a polyhedral mesh created by planar triangles representing a subdivision of an initial icosahedron or octahedron grids. Numerical experiments illustrate the behaviour of each proposed filter on artificial data and on real measurements, namely the GOCE satellite observations, which represent second derivatives of gravity potential, and the satellite-only mean dynamic topography data, which represent changes of the water mass in Earth's oceans.

Keywords: data filtering, nonlinear diffusion equation, mean curvature flow, geodetics mean curvature flow, surface finite volume method, GOCE data, satellite-only mean dynamic topography

Abstrakt

Dizertačná práca pojednáva o filtračných metódach určených na spracovanie geodetických dát na uzavretých plochách. Tieto metódy sú založené na lineárnych, nelineárnych a geometrických difúznych rovniciach. Lineárna difúzia na ploche je definovaná pomocou Laplace-Beltramiho operátora, ktorý predstavuje zovšeobecnenie Laplaceovho operátora na plochách. V práci je použitá metóda založená na Perona-Malikovom modeli, v ktorej je difúzny koeficient závislý od povrchových gradientov dát a predstavuje sa nový model nelineárnej difúzii, ktorý je závislý od povrchového Laplaceovho operátora aplikovaného na filtrované dáta. Tieto modely umožňujú adaptívnu filtráciu, teda filtráciu, ktorá zachováva dôležité štruktúry v dátach, ako napríklad hranice štruktúr či lokálne extrémy dát. Adaptívnu filtráciu je možné dosiahnuť použitím rovníc založených na nelineárnej geometrickej difúzii. Takáto difúzia je riadená vývojom izočiar pomocou strednej krivosti. Na numerickú aproximáciu uvedených parciálnych diferenciálnych rovníc bola použitá povrchová metóda konečných objemov. Samotná výpočtová oblasť je aproximovaná trianguláciou, ktorá vznikla delením pôvodnej icosahedronovej a octahedronovej siete. V práci sa vyskytuje niekoľko numerických experimentov, ktoré skúmajú vlastnosti jednotlivých metód, ale aj experimenty, v ktorých sú spracovávané reálne geodetické údaje. Konkrétne sú v práci filtrované satelitné dáta z družice GOCE, ktorá meria druhé derivácie gravitačného potenciálu a satelitné dáta strednej dynamiky topografie oceánov (ang. mean dynamic topography), ktoré popisujú zmenu hmôt vo svetových oceánoch.

Kľúčové slová: filtrácia dát, nelineárne diffúzne rovnice, vývoj podľa strednej krivosti, geodetická stredná krivosť, povrchová metoda konečných prvkov, GOCE dáta

Contents

Chapter 1

Introduction

In many applications, it is necessary to analyse data, e.g. classical images given on 2D or 3D regular grid structure or geoscience data given on 2D surfaces like the Earth topography or satellite orbits, which are often contaminated by noise, and their quality can be rather poor. Nonlinear partial differential equations (PDEs) can be used to automatically produce an output of higher quality, enhance the sharpness, filter out the noise, extract shapes, etc. From the mathematical point of view, the input processed data can be modelled by a real function $u^0(x)$, $u^0 : \Omega \to R$, where $\Omega \subset R^d$ represents a spatial domain. In image analysis, Ω is typically rectangular and $d = 2$ or 3, in surface data analysis Ω is a closed or open surface in R^3. In the presented approach we are strongly inspired by ideas from classical image processing which we transfer to geodesy surface data analysis. Image processing operations based on PDEs involve such important tasks as image filtering, edge detection, deblurring and image enhancement, restoration, image inpainting, shape extraction and analysis, image segmentation, motion analysis, motion based filtering etc.[1, 2, 3, 4, 5, 6, 7, 8, 9].

The first step to use PDEs for image processing was done in the beginning of eighties [10, 11]. By the simple observation that the Gauss function

$$G_\sigma(x) = \frac{1}{(4\pi\sigma)^{d/2}} e^{-|x|^2/4\sigma} \tag{1.1}$$

is the fundamental solution of the linear heat (diffusion) equation, it has been possible to replace the classical image processing operation – convolution of an image with the Gauss kernel (normal probability distribution function) with variance $v = \sqrt{2\sigma}$ (Gaussian smoothing) – by solving the linear heat (diffusion) equation

$$u_t = \Delta u \tag{1.2}$$

for time $t = \sigma$ with initial condition given by the processed image u^0. Here Δ denotes the classical Laplace operator in cartesian coordinates and u_t denotes the time derivative of the unknown function $u(t,x)$, $u : [0,T] \times \Omega \to R$.

It is well known that Gaussian smoothing (linear diffusion) blurs edges and moves their positions in images as well as smooths out local extrema of data. Although such phenomena can cause no problems in some examples of data analysis, in applications where, e.g., a visual impression is crucial and a precise localization of edges and values at extrema are necessary, the linear (Gaussian) smoothing is generally not the best choice. A way has been found to overcome these shortcomings, namely to switch to nonlinear diffusion models.

Due to the evolutionary character of the process which controls the processing using diffusion equations, application of any PDE to an initially given image is understood as its embedding in the so-called *scale space*. The Gaussian smoothing represents *linear scale space*. In the case of nonlinear PDEs, one speaks about *nonlinear scale space*. The axioms and fundamental properties of such embeddings have been summarized and studied by Alvarez, Guichard, P.L. Lions and Morel in [1, 2, 12], where the notion of *image multiscale analysis* has been introduced. The image multiscale analysis associates with a given image $u^0(x)$ a family $u(t,x)$ of smoothed-simplified images depending on an abstract parameter $t \in [0,T]$, the *scale*. As has been proved in [1], if such a family fulfills certain basic assumptions – pyramidal structure, regularity and local comparison principle – then $u(t,x)$, $u : [0,T] \times \Omega \to R$, can be represented as the unique viscosity solution (in the sense of

[13]) of a general second order (degenerate) parabolic partial differential equation.

Since the end of the 80s, the nonlinear diffusion equations have been used for processing of 2D and 3D images. After the pioneering work of Perona and Malik [14] who modified the linear heat equation (1.2) to nonlinear diffusion preserving edge positions, there has been a great deal of interest in the application and analysis of such equations. At present, the following nonlinear PDE suggested by Catté, P.L.Lions, Morel and Coll [15], often called regularized Perona-Malik model, is widely used in various practical image processing applications:

$$u_t - \nabla.(g(|\nabla G_\sigma * u|)\nabla u) = 0, \tag{1.3}$$

where $u(t,x)$ is an unknown function. The equation is accompanied by the zero Neumann boundary conditions, the initial condition is given by the processed image $u^0 \in L_\infty(\Omega)$, the following assumptions on diffusion coefficient function g and smoothing kernel G_σ are prescribed

$$g : R_0^+ \to R^+ \text{ is a nonincreasing function}, g(0) = 1, g(s) \to 0 \text{ for } s \to \infty, \tag{1.4}$$

$$G_\sigma \in C^\infty(R^d) \text{ is a smoothing kernel}, \int_{R^d} G_\sigma(x)\,dx = 1, \int_{R^d} |\nabla G_\sigma|\,dx \le C_\sigma, \tag{1.5}$$

$$G_\sigma(x) \to \delta_x \text{ for } \sigma \to 0, \text{ where } \delta_x \text{ is Dirac function localized at point x}, \tag{1.6}$$

and

$$\nabla G_\sigma * u(x) = \int_{R^d} \nabla G_\sigma(x-\xi)\tilde{u}(\xi)\,d\xi, \tag{1.7}$$

where $\tilde{u}$ is an extension of u to R^d. One can consider the extension of u by 0 outside Ω or the reflective periodic extension of the image [15].

The equation (1.3) represents a modification of the original Perona-Malik model [14, 16, 17]

$$u_t - \nabla.(g(|\nabla u|)\nabla u) = 0, \tag{1.8}$$

called also *anisotropic diffusion* in the computer vision community. Perona and Malik introduced (1.8) in the context of edge enhancement. The equation selectively diffuses the image in the regions where the signal has small variance in intensity in contrast with those regions where the signal changes its tendency. Such a diffusion process is governed by the shape of the diffusion coefficient given by the function g in (1.8) and by its dependence on ∇u, which is understood as an edge indicator [14]. Since $g \to 0$ for large gradients, the diffusion is strongly slowed down on edges, while outside them it provides averaging of pixel intensities as in the linear case. From a mathematical point of view, for practical choices of g (e.g. $g(s) = 1/(1+s^2)$, $g(s) = e^{-s^2}$), the original Perona-Malik equation (1.8) can behave locally like the backward heat equation. It is, in general, an ill-posed problem which suffers from non-uniqueness and whose solvability is a difficult problem [17]. One way to overcome this disadvantage was proposed in [15], where the convolution with the Gaussian kernel G_σ was introduced into the decision process for the value of the diffusion coefficient, cf. (1.3). Since convolution with the Gaussian is equivalent to linear diffusion, their model combines ideas of linear and nonlinear scale space equations. Such a slight modification made it possible to prove the existence and uniqueness of solutions for the modified equation, and to keep the practical advantages of the original formulation [15]. Moreover, usage of the *Gaussian gradient* $\nabla G_\sigma * u$ combines the theoretical and implementation aspects of the model. The convolution (with prescribed σ) gives a unique way to compute gradients of a piecewise constant image. It also bounds (depending on σ) the gradient of the solution as an input of the function g in the continuous model – which corresponds to the situation in numerical implementations where gradients evaluated on a discrete grid are finite. Also, the local edge enhancement is more understandable in the presence of noise.

In the thesis we present linear and nonlinear diffusion filtering methods for geodesy data given on closed surfaces. For readers interested in image processing numerical algorithms on regular grids we refer, e.g., to [18, 19] and further references therein. In order to process surface data by PDEs like (1.2) and (1.3), instead of standard gradient and Laplacian, we have to consider the surface gradient and surface Laplacian – so called Laplace-Beltrami operator. For any scalar function u defined on an open subset G of R^d containing surface Ω

the surface (tangential) gradient is defined by

$$\nabla_s u = \nabla u - (\nabla u \cdot \nu)\nu, \tag{1.9}$$

where ν is outer unit normal to the closed surface Ω and ∇u denotes the usual gradient and $\cdot$ denotes the usual scalar product on R^d. The tangential gradient $\nabla_s u$ only depends on the values of u restricted to surface Ω and $\nabla_s u \cdot \nu = 0$. The Laplace-Beltrami operator on surface Ω is then defined as the tangential divergence of the tangential gradient, i.e.

$$\Delta_s u = \nabla_s \cdot \nabla_s u. \tag{1.10}$$

We also recall the Green (integration by parts) formula for scalar functions on surfaces and its consequences [20, 21, 22], which will be used in derivation of numerical schemes later in the thesis. Let Γ be a subset of Ω having a boundary $\partial\Gamma$ whose unit outer normal, tangential to Γ, is denoted by η. Then

$$\int_\Gamma \nabla_s u \, dA = \int_{\partial\Gamma} u\eta \, da - \int_\Gamma H u \nu dA, \tag{1.11}$$

where H denotes the (scalar) mean curvature of Γ, and dA denotes 2D surface element measure and da denotes 1D curve element measure, for the proof see [22], Theorem 2.10. Let q be a tangential vector field to the surface Γ, i.e. $q \cdot \nu = 0$, a typical example used later is the so called surface diffusion flux given by $q = g\nabla_s u$, where g is a scalar function defined on the surface. Then from (1.11) we obtain divergence theorem on the surface

$$\int_\Gamma \nabla_s \cdot q \, dA = \int_{\partial\Gamma} q \cdot \eta \, da - \int_\Gamma H q \cdot \nu dA = \int_{\partial\Gamma} q \cdot \eta \, da. \tag{1.12}$$

and choosing $g = 1$ in surface diffusion flux we get

$$\int_\Gamma \Delta_s u \, dA = \int_{\partial\Gamma} \nabla_s u \cdot \eta \, da. \tag{1.13}$$

The content of the thesis is organized into four main chapters. The chapter 2 is dedicated to the linear diffusion filter on a closed surface and it is divided into two sections. The section 2.1 presents numerical discretization of linear diffusion on a closed surface, while the section 2.2 study a uniform filtering behaviour of the model on the testing experiment. The chapter 3 presents different filters, which are based on the nonlinear diffusion on a closed surface. Namely, the section 3.1 is dedicated to the numerical discretization of the regularized surface Perona-Malik model and the section 3.2 represents adaptive filtering behaviour of the model. A new approach in filtering methods represents the nonlinear diffusion influenced by the surface Laplacian. The idea of this approach is based on the drawback of the regularized Perona-Malik model in the area of local extrema of data. A numerical approximation of the model is the main topic of sections 3.3. Consequently, the section 3.4 presents testing experiment, where we compare the efficiency of the new method with linear and nonlinear regularized Perona-Malik model. The chapter 4 introduces the nonlinear geometrical diffusion filter on a surface. The section 4.1 deals with a numerical approximation of the mean curvature flow equation on the closed surface and in the section 4.2 we describe the approximation of surface geodesic mean curvature flow on the same domain. The behaviour of both models is illustrated in the section 4.3. This section presents two testing numerical experiments, which study a behaviour of the model with different input parameters and we compare the filtering effect with the other nonlinear diffusion models. The next chapter deals with numerical experiments on filtering of real geodetic data. Namely, the chapter 5 presents filtering of the components of the GOCE gravity gradients tensor in two different referential systems, the satellite-only mean dynamic topography data, which represent dynamic of mass in the Earth's ocean. The last chapter presents short conclusions of the thesis and possibilities of the further research.

Chapter 2

The linear diffusion filter on a surface

The linear diffusion of a scalar function u on a closed surface Ω is given by the equation

$$\partial_t u = \Delta_s u, \tag{2.1}$$

which is a direct generalization of equation (1.2) and serves for a uniform smoothing of data on surfaces. Since the surface is closed, no boundary conditions have to be prescribed. Processed data $u^0(x)$ defined on Ω gives initial condition for (2.1).

2.1 Numerical discretization of linear diffusion on a surface

The differential equation (2.1) is numerically solved by the surface finite volume method [23, 24, 25]. In this approach, the surface Ω is approximated by an appropriate triangulation defined by N representative nodes $X_i, X_i \subset \Omega, i = 1, \ldots, N$. These nodes represent vertices of the triangular grid defined by planar triangles $T_{iq}, q = 1, ..., Q_i, i = 1, ..., N$, where Q_i is the number of triangles with the vertex X_i. Other two vertices of the triangle T_{iq} will be denoted by X_i^{q1} and X_i^{q2}. A value of function u in the node X_i is denoted by u_i. For the given triangulation we construct a finite volume grid. At each node X_i we create a co-volume (finite volume) V_i bounded by straight lines that connect midpoints between X_i and its neighbours X_i^{q1}, X_i^{q2} with centers of mass of all triangles joined in the node X_i. By integrating equation (2.1) over the finite volume V_i , by applying (1.13) to its right hand side and taking into account geometry of the boundary of co-volume we obtain

$$\int_{V_i} \partial_t u \, dA = \sum_{q=1}^{Q_i} \int_{\partial V_{iq}} \nabla_s u \cdot \vec{\eta}_{iq} da, \tag{2.2}$$

where $\nabla_s u$ represents the surface gradient of the function u and ∂V_{iq} are parts of the co-volume boundary that belong to T_{iq} having outer normal vectors $\vec{\eta}_{iq}$.

Eq. (2.1) is solved in a time interval $[0, T]$. This interval is divided into M time steps t_j, $j = 1, \ldots, M$ and the time derivative $\partial_t u$ is approximated by the backward difference. Then we get

$$m(V_i) \frac{u_i^j - u_i^{j-1}}{\tau} = \sum_{q=1}^{Q_i} \int_{\partial V_{iq}} \nabla_s u^j \cdot \vec{\eta}_{iq} da. \tag{2.3}$$

where $m(V_i)$ denotes the area of co-volume V_i and $\tau = t_j - t_{j-1}$ denotes the time step and the value of u^j represents a solution in the j^{th} time step.

For the right hand side of Eq. (2.3) let us consider a linear representation of u^j on each triangle. Then the surface gradient $\nabla_s u^j$ is a constant vector over each triangle T_{iq} and we can replace it by the mean value

$$\nabla_s u^j = \frac{1}{m(T_{iq})} \int_{T_{iq}} \nabla_s u^j da, \tag{2.4}$$

where $m(T_{iq})$ denotes the area of the triangle T_{iq}. Applying (1.11) to the right hand side of Eq. (2.4), since any triangle has the zero mean curvature, we obtain

$$\nabla_s u^j = \frac{1}{m(T_{iq})} \int_{\partial T_{iq}} u^j \cdot \vec{n}_{iq} da, \tag{2.5}$$

where $\vec{n}_{iq}$ is the unit outer normal vector, tangential to the boundary of the triangle T_{iq}. For the linear representation of u^j, the integral over the triangle boundary can be expressed as a sum of average values from each triangle side, and denoting by $\vec{P}^j_{T_{iq}}$ the constant approximation of the surface gradient on the triangle T_{iq}, we get

$$\vec{P}^j_{T_{iq}} = \frac{1}{m(T_{iq})} \left(\frac{u^j_i + u^j_{q1}}{2} d_{iq1}\vec{n}_{iq1} + \frac{u^j_i + u^j_{q2}}{2} d_{iq2}\vec{n}_{iq2} + \frac{u^j_{q1} + u^j_{q2}}{2} d_{q1q2}\vec{n}_{q1q2} \right) \tag{2.6}$$

where $u^j_i, u^j_{q1}, u^j_{q2}$ denotes the nodal values of the solution in triangle nodes X_i, X_i^{q1}, X_i^{q2}. Consequently, the approximation of Eq. (2.3) can be written in the form

$$m(V_i)\frac{u^j_i - u^{j-1}_i}{\tau} = \sum_{q=1}^{Q_i} \int_{\partial V_{iq}} \vec{P}^j_{T_{iq}} \cdot \vec{\eta}_{iq} da. \tag{2.7}$$

Since $\vec{P}^j_{T_{iq}}$ is a constant vector and

$$\int_{\partial V_{iq}} \vec{\eta}_{iq} = m(e^1_{iq})\vec{\eta}^1_{iq} + m(e^2_{iq})\vec{\eta}^2_{iq}, \tag{2.8}$$

where $m(e^1_{iq})$ and $m(e^2_{iq})$ are lengths of the parts of the co-volume boundaries inside the triangle T_{iq}, we get

$$m(V_i)\frac{u^j_i - u^{j-1}_i}{\tau} = \sum_{q=1}^{Q_i} \left[m(e^1_{iq})\vec{\eta}^1_{iq} \cdot \vec{P}^j_{T_{iq}} + m(e^2_{iq})\vec{\eta}^{2,}_{iq} \cdot \vec{P}^j_{T_{iq}} \right] \tag{2.9}$$

which can be, for every $i = 1, ..., N$, written in the form

$$u^j_i - \frac{\tau}{m(V_i)} \sum_{q=1}^{Q_i} \left[m(e^1_{iq})\vec{\eta}^1_{iq} \cdot \vec{P}^j_{T_{iq}} + m(e^2_{iq})\vec{\eta}^{2,}_{iq} \cdot \vec{P}^j_{T_{iq}} \right] = u^{j-1}_i \tag{2.10}$$

and represents the implicit numerical scheme for solving linear diffusion equation (2.1) on the closed surface Ω.

Eqs. (2.10) represent a linear system of equations which can be written in the form

$$\vec{A}\vec{u}^j = \vec{u}^{j-1} \tag{2.11}$$

where $\vec{A}$ represents the system matrix and $\vec{u}^j = [u^j_1, ..., u^j_N]^T$ is a vector of nodal values of the solution in the j^{th} time step. The system matrix $\vec{A}$ is a sparse non-symmetric matrix and its properties depend on the time step τ and geometry of the triangulation. Let us define a local numbering of nodal values in co-volume and its neighbourhood: the nodal value in the co-volume centre will be denoted by u^j_{i0} and its neighbouring unknown values are denoted by $u^j_{i1}, ..., u^j_{iQ_i}$. Then the equation corresponding to co-volume V_i contains $Q_i + 1$ unknowns $u^j_{i0}, u^j_{i1}, ..., u^j_{iQ_i}$ and i^{th} row of the linear system (2.11) is given by

$$\sum_{q=0}^{Q_i} a^j_{iq} u^j_{iq} = u^{j-1}_{i0}, \tag{2.12}$$

where $a^j_{i0}, a^j_{i1}, ..., a^j_{iQ_i}$ represent non-zero coefficients in the i^{th} row of the matrix $\vec{A}$ (let us note that for the linear diffusion approximation the upper (time) index j is dummy, but it will play a role in nonlinear diffusion approximation later). The exact column locations of these non-zero coefficients depends on a global indexing of the corresponding nodal value.

2.2 Behaviour of the linear diffusion on a closed surface

In this section, we present a simple numerical experiment showing how an additive noise is filtered from an artificial function defined on a computational domain. To approximate a sphere with the chosen radius $r = 1000$ we use the 9^{th} subdivision of the initial icosahedral grid. In this experiment we use the triangulation with 655 362 nodes and 1 310 720 triangles. On this triangulated sphere we defined an artificial piecewise constant function w in such a way that $w_i = 1$ for all nodes located on lands and $w_i = 0$ for all nodes at oceans. Onto this function w we put an additive noise at 130 697 nodes which represent approximately 20% of all nodes randomly distributed over the sphere. The generated uniform non-Gaussian additive noise is from the interval $(-0.3, 0.4)$ and after adding the noise we get our initial condition u^0 for which $u_i^0 \in (0.7, 1.4)$ on lands and $u_i^0 \in (-0.3, 0.4)$ at oceans (Fig. 2.1 left). The system of linear equations (2.11) has to be solved in every filtering (time) step. To that goal, in numerical experiments, we use the SOR (successive-over-relaxation) method [26] or BiCGSTAB (biconjugate gradient stabilized) method [27]. In order to get convergence of SOR, we make the system matrix diagonally dominant choosing the time step τ proportional to an average area of the co-volumes [23, 24]

$$\tau = \frac{1}{N} \sum_{i=1}^{N} m(V_i)\,. \tag{2.13}$$

The choice of the time step is essential for the whole filtering process and implies how many filtering (time) steps (we call it also iterations) will be necessary to get reasonable results. For the better description of the behaviour of the linear model, we use in this experiment smaller time step $\frac{1}{10}\tau$. Such a selection of smaller time step can describe the evolution of the solution more specifically. In this experiment, the function which has to be reconstructed is known, therefore we are able to demonstrate the behaviour of the linear diffusion model. In each time step, we compute the root mean square (RMS) of residuals according to the formula

$$RMS = \frac{1}{N} \sqrt{\sum_{i=1}^{N} (w_i - u_i)^2}. \tag{2.14}$$

The minimal RMS is obtained from the solution in the second time step and reaches a value 0.0673 and then the RMS grows. Fig. 2.1 (right) shows profiles from solutions obtained after 2, 5 and 10 iterations of the linear diffusion filtering ($\tau = 1.921$) along the equator across South America. From the result, it is evident that this approach reduces the additive noise but it has a uniform smoothing effect comparable to other linear filters. This can produce serious inaccuracies in the interpretation of processed data. A way how to avoid such inaccuracies is to use nonlinear filtering methods.

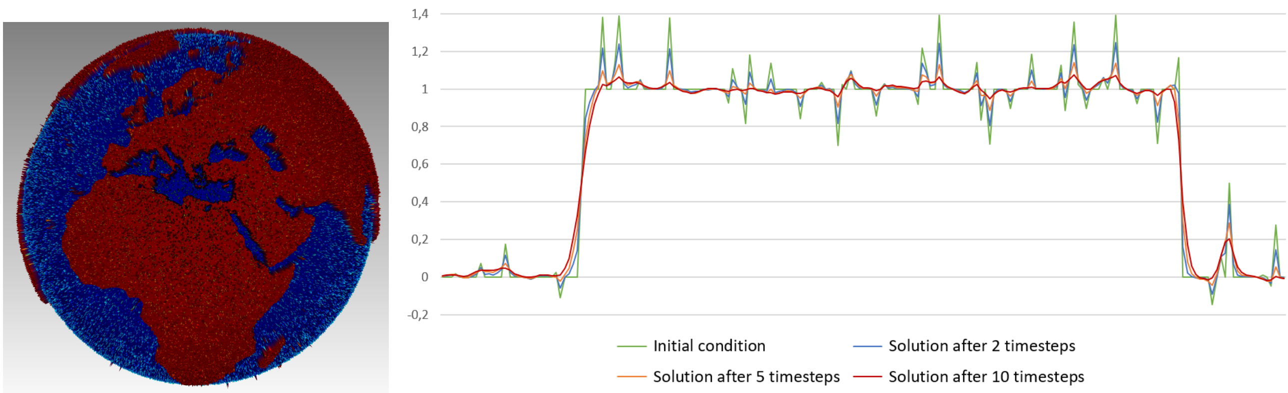

Figure 2.1: The initial condition u^0 (left), profiles across South America from the solution of filtering of noise using the surface linear diffusion after 2, 5 and 10 time steps (right)

Chapter 3

The nonlinear diffusion filter on a surface

To perform a nonuniform smoothing of data on surfaces we need to choose an appropriate diffusion coefficient in diffusion PDEs. The main idea is that the diffusion coefficient should not be a constant but a nonlinear function of differential characteristics of data. The important feature of linear and the nonlinear diffusion is that they both have a property that they conserve an average value of data during the filtering. In following sections, we present numerical approximations of different nonlinear models with their corresponding nonlinear diffusion functions, namely the regularized surface Perona-Malik model and the nonlinear diffusion model influenced by the surface Laplacian.

3.1 The regularized surface Perona-Malik model

In this approach, originally developed in [23], we use an analogy with the regularized Perona-Malik model (1.3) from the classical image processing and we suggest following PDE

$$\partial_t u = \nabla_s \cdot (g(|\nabla_s u^\sigma|)\nabla_s u) \tag{3.1}$$

for filtering the data on surfaces. The nonlinear diffusivity function g depends on the term $\nabla_s u^\sigma$, the surface gradient of solution u smoothed by the surface linear diffusion for a short time interval σ, and represents an edge detector for surface data. We consider g in the form

$$g(|\nabla_s u^\sigma|) = \frac{1}{1 + H|\nabla_s u^\sigma|^2}, \quad H \geq 0, \tag{3.2}$$

where constant H represents an edge sensitivity parameter. By this definition, g fulfils assumption (1.4) and returns values from the range $0 < g(|\nabla_s u^\sigma|) \leq 1$.

The parameter H determines how sensitive will be the edge detector to high values of a smoothed surface gradient of u and gives us a decision capability which gradients to preserve. Large gradients which represent edges in processed data yield a small value of edge detector and vice versa. If the values of edge detector are close to zero, the diffusion process is strongly slowed down, on the other hand, if the values are close to 1, the process is similar to the linear diffusion. This allows the adaptive smoothing according to surface gradients of the solution. The parameter σ affects the solution u^σ of the surface linear diffusion from which the surface gradient is computed. This pre-smoothing of surface gradients causes that only un-noisy edges will be preserved in the nonlinear adaptive smoothing process. An appropriate choice of the parameters H and σ plays an important role in the filtering process and needs to be tuned experimentally.

To approximate the Eq. (3.1) we use analogous steps as described in section 2.1 we obtain the numerical scheme

$$u_i^j - \frac{\tau}{m(V_i)} \sum_{q=1}^{Q_i} \left[m(e_{iq}^1)\vec{\eta}_{iq}^1 \cdot \vec{P}_{T_{iq}}^j g(|\vec{P}_{T_{iq}}^{\sigma,j-1}|) + m(e_{iq}^2)\vec{\eta}_{iq}^{2,} \cdot \vec{P}_{T_{iq}}^j g(|\vec{P}_{T_{iq}}^{\sigma,j-1}|) \right] \;=\; u_i^{j-1}, \tag{3.3}$$

$i = 1, ...N$, which represents a semi-implicit numerical scheme for solving the regularized Perona-Malik model on the closed surface Ω. The diffusivity function g inside the scheme (3.3) depends on $P_{T_{iq}}^{\sigma,j-1}$ that represents numerical approximation of the surface gradient on triangle T_{iq} of the solution u at the previous time step $j-1$ smoothed by one step σ of the surface linear diffusion. In such a way the nonlinearity in the equation (3.1) is treated by using the smoothed gradients from the previous time step, thus leading to the system of linear equations. Comparing the semi-implicit scheme (3.3) with the implicit scheme (2.10) for the surface linear diffusion, the difference is that now the surface gradients $P^j_{T_{iq}}$ are multiplied by the edge detector function g which allows the adaptive smoothing according to the smoothed surface gradients evaluated at the previous time step. Consequently, the edge detector is step by step evolving in time giving an opportunity to preserve main structures in the data and effectively reduce the noise.

Our experience shows that the regularized surface Perona-Malik model (3.1) successfully reduces noise while preserves edges, but we have also observed that it slightly smooths out local extrema of filtered data [23, 24]. It is due to the fact that the smoothed surface gradients are not high enough in areas of local extrema, but opposite, they are close to zero.

3.2 The behaviour of the regularized surface Perona-Malik model

To show behaviour and advantages of the nonlinear diffusion model (3.1) we use the same experiment as we used in section 2.2. This experiment aims to demonstrate how diffusion filtering controlled by the edge detector can successfully remove an additive noise. We use the same space discretization of the unit sphere and the same initial condition (Fig. 2.1 left). In case of the nonlinear surface diffusion, the linear system of equations is given by the semi-implicit scheme (3.3). To get this system, first, we have to apply the linear diffusion filtering to the solution from the previous time step. Then we evaluate the corresponding surface gradients that indicate values of the edge detector. After that, we are able to compute coefficients of the system matrix. This process is repeated in every filtering step. Therefore, the nonlinear surface diffusion filtering is more time consuming and usually requires more iterations than the linear one.

A significant part of data filtering is finding the optimal values for the edge detector function parameters H and σ and the time step τ and the number of iterative (filtering) time steps. Since in this experiment the true (unnoisy) solution is known, we are able to tune the parameters considering the RMS of residuals between the true and filtered solutions (2.14). In general, the parameters for the edge detector depend on gradients of processed data. To describe the influence of the sensitivity parameter to the model, we use several different values of this parameter and we compute the RMS of residual for each selection. The minimal RMS of residuals is decreasing along with increasing value of H, but also along with increasing numbers of time steps. The difference between the minimal RMS of residuals obtained using $H = 35\ 000$ and $H = 65\ 000$ is smaller than 0.001, while the number of time steps required to obtain the minimal RMS in the case of $H = 65\ 000$ is almost 81% higher. see Fig. 3.1 (right). Fig. 3.1 (left) depicts profiles from the solution of filtering after 15, 52 and 100 iterations of the nonlinear diffusion along the equator across South America using $H = 35\ 000$. From the result, it is evident that the signal corresponding to the additive noise is step by step vanishing while high gradients and their positions remain preserved. Here we remind that the edge detector always depends on surface gradients computed from the solution in the previous iterative step, thus it is adapted to the filtered solution evolving in time. Such an adaptive smoothing effect is a main advantage of the nonlinear filtering.

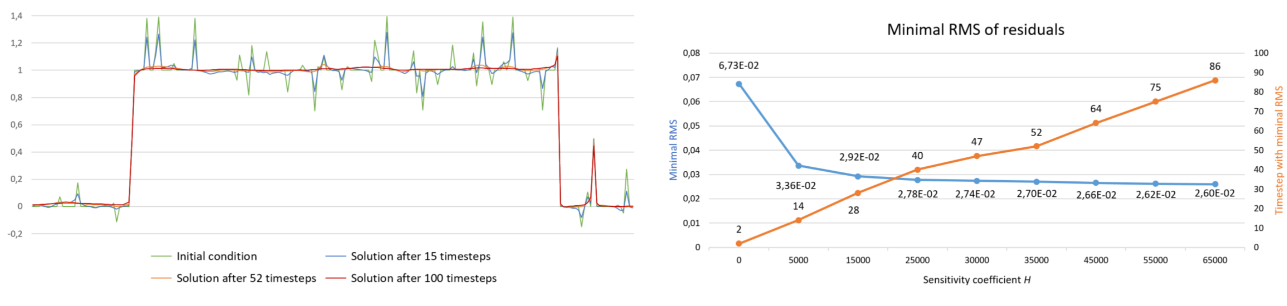

Figure 3.1: Profiles across South America from the solution of filtering of the additive noise using the surface Perona-Malik diffusion after 15, 52 and 100 time steps (left), the minimal RMS of residuals (with corresponding number of time step) for different selections of the parameter H (right)

3.3 The nonlinear diffusion influenced by the surface Laplacian

In this section, we present an extension of the edge detector function of the Perona-Malik model by another argument which will slow down diffusion process in areas of local extrema, i.e. in regions with large values of surface Laplacian – the Laplace-Beltrami operator [24]. The diffusion coefficient which represents the edge and local extrema detector is defined by

$$g(|\nabla_s u^{\sigma_1}|, \Delta_s u^{\sigma_2}) = \frac{1}{1 + H_1|\nabla_s u^{\sigma_1}|^2 + H_2(\Delta_s u^{\sigma_2})^2}, H_1, H_2 \geq 0. \tag{3.4}$$

The function g depends on the surface gradient of the solution u smoothed by the linear diffusion equation for a time interval σ_1 as well as on the Laplace-Beltrami operator applied to solution u smoothed by the linear diffusion equation for a time interval σ_2. The parameter H_1 has the same meaning as in the edge detector in the regularized Perona-Malik model and the parameter H_2 affects sensitivity to high values of the surface Laplacian of the function u. Alternatively, we can use diffusivity coefficient g in the form

$$g(\Delta_s u^{\sigma}) = 1 - \frac{1}{1 + H(\Delta_s u^{\sigma})^2}, H \geq 0. \tag{3.5}$$

In this case, the function (3.5) speeds up the diffusion in extremal values and we found that this choice of the diffusivity function is useful in the case of extremal noise. Experimentally we have found that by applying few steps of diffusion filtering based on this function and afterwards to use a different nonlinear model, we can better preserve structures of processed data.

To obtain the numerical schemes of the nonlinear diffusion models influenced by the surface Laplacian in forms

$$\partial_t u = \nabla_s \cdot (g(|\nabla_s u^{\sigma_1}|, \Delta_s u^{\sigma_2})\nabla_s u), \tag{3.6}$$

$$\partial_t u = \nabla_s \cdot (g(\Delta_s u^{\sigma_2})\nabla_s u), \tag{3.7}$$

we need to approximate the value of the Laplace-Beltrami operator on the triangle of co-volume.

To approximate the Laplace-Beltrami operator we use numerical approximation of the surface linear diffusion. Then we can denote the approximated mean value on the co-volume V_i in time step j by C_i^j and we obtain

$$C_i^j = \frac{1}{m(V_i)} \sum_{q=1}^{Q_i} \left[m(e_{iq}^1)\vec{\eta}_{iq}^1 \cdot \vec{P}_{T_{iq}}^j + m(e_{iq}^2)\vec{\eta}_{iq}^{2,} \cdot \vec{P}_{T_{iq}}^j \right], \tag{3.8}$$

which can be also understood as an approximation of the Laplace-Beltrami operator in the vertex X_i^j. Since we need a value of diffusion coefficient on the edges of co-volume, i.e. on the triangles meeting in the center of co-volume, we compute the average value of the Laplace-Beltrami operator on the triangle T_{iq} by

$$C_{T_{iq}}^j = \frac{1}{3}(|C_i^j| + |C_{q1}^j| + |C_{q2}^j|), \tag{3.9}$$

where C_i^j, C_{q1}^j and C_{q2}^j represent the values in triangle vertices.

Using the same approach as we have used in the section 2.1, we obtain a semi-implicit numerical scheme for the nonlinear diffusion filtering method influenced by the surface Laplacian on the closed surface Ω

$$\begin{aligned} u_i^j - \frac{\tau}{m(V_i)} \sum_{q=1}^{Q_i} \Bigg[& m(e_{iq}^1)\vec{\eta}_{iq}^1 \cdot \vec{P}_{T_{iq}}^j g(|\vec{P}_{T_{iq}}^{\sigma_1, j-1}|, |C_{T_{iq}}^{\sigma_2, j-1}|) \\ & + m(e_{iq}^2)\vec{\eta}_{iq}^{2,} \cdot \vec{P}_{T_{iq}}^j g(|\vec{P}_{T_{iq}}^{\sigma_1, j-1}|, |C_{T_{iq}}^{\sigma_2, j-1}|) \Bigg] \quad = \quad u_i^{j-1}, \end{aligned} \tag{3.10}$$

$i = 1, ..., N$, where $\vec{P}_{T_{iq}}^{\sigma_1, j-1}$ is an approximation of the smoothed gradient of the solution from the previous time step $j-1$, and analogously, $C_{T_{iq}}^{\sigma_2, j-1}$ is an approximation of the smoothed surface Laplacian of the solution from the previous time step $j-1$.

3.4 The behaviour of the nonlinear diffusion influenced by the surface Laplacian

In this section we use the nonlinear diffusion model influenced by the surface Laplacian with edge and extrema detector function (3.4). To get the linear system of the equations given by the semi-implicit scheme (3.10), we need to apply the linear diffusion filtering more than once. At first, we need to apply the linear diffusion with σ_1 to the solution from the previous time step, and then we evaluate the corresponding surface gradients. Secondly, we need to apply again the linear diffusion to the solution from the previous time step, but in this case, we need to use σ_2. Subsequently, we evaluate the surface Laplacian and then, we get the values of the edge and extrema detector function.

To compare this new approach with surface Perona-Malik model, we use the same sensitivity coefficient $H_1 = 35\,000$ for the edge detection as we use in section 3.2. Consequently, we use several sensitivity coefficients H_2 and we compute the RMS of residuals (2.14) for each selection. Fig. 3.2 (left) shows the minimal RMS for each selection of H_2. In this experiment we use $\sigma_1 = \tau$ and $\sigma_2 = \frac{1}{10}\tau$. The parameter σ_2 is notably smaller since we need to preserve high values of surface Laplacian in local extrema. As we can see in the figures, the minimal RMS of residual is decreasing along with increasing H_2. The difference between the minimal RMS of residuals obtained by this approach and the one obtained by the surface Perona-Malik model is higher than $0.29 \cdot 10^{-2}$ (using $H_2 = 15\,000$). However, it should be noted that we need 28 more time steps to achieve this minimal RMS. Fig. 3.2 (right) depicts differences between the solutions obtained by the surface Perona-Malik model and by the extended model after 80. Both solutions are from the same time step using $H = H_1 = 35\,000$ and $H_2 = 15\,000$. In the figure, we can see that the extremal differences are in the nodes which represent island structures (local extrema). From the behaviour of these differences, we can conclude that the nonlinear diffusion influenced by the surface Laplacian preserves these structures better.

In the second part of the experiment, we focus on the behaviour of the nonlinear extrema reduction model with extrema detector function (3.5). At first, we need to modify an artificial noise of the experiment. To each node affected by the noise, we add a random number from the range of $(-1,1)$. Such an adjustment extends the interval of u^0 to $(-1.3, 2.4)$. This modification is important for a correct interpretation of the behaviour of the model since it is suitable only for a reduction of an extremal noise, which must be significantly higher than the original piecewise constant function w. If we want to use the surface Perona-Malik model for this modified experiment, we must use higher σ for the linear pre-filtration. This can result in the movement of the initial border structures in the surface gradient computation. We can avoid such a disadvantage using the nonlinear extrema reduction model. As the model parameters we use $H = 10$ and $\sigma = 0.01$. Results shows that the initial interval of data shrinks to $(-0.52, 1.54)$ while the RMS of residuals decreases from the initial value 0.35 to 0.143. So it is evident that the model successfully reduces the extremal noise to smaller amplitudes. After this reduction, we can use a different nonlinear diffusion model to get the precise solution (e.q. surface Perona-Malik model).

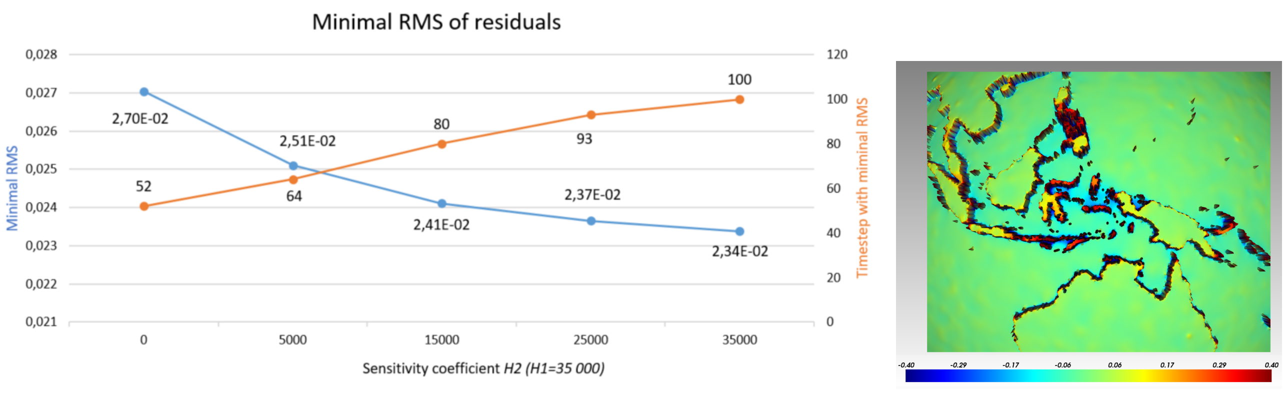

Figure 3.2: The minimal RMS of residuals (with the corresponding number of time step) for different selections of the parameter H_2 (left), differences from the solution of surface Perona-Malik model (right)

Chapter 4

The nonlinear geometrical diffusion filter on a surface

A different type of surface filters represents the nonlinear filters based on the geometrical diffusion. In general, a scalar function u which represents processed data can be represented by a set of specific contour lines. A properly designed evolution of these contour lines corresponds to the smoothing of processed data. This type of equations is known as nonlinear PDEs of a mean curvature flow type [28, 29, 9, 3]. The evolution in the normal direction, which depends on curvature is given by PDE in the level set formulation in the form

$$\partial_t u = |\nabla u| \nabla \cdot \left(g \frac{\nabla u}{|\nabla u|} \right). \tag{4.1}$$

In the case of $g = 1$, this equation represents the mean curvature flow (MCF) which is also known as a curvature filter. Such level set model performs uniform intrinsic smoothing of all contour lines at ones. And it is fast if the curvature of contour lines is high – contour lines of noise – while the evolution of the other contour lines is slower. For the edge-preserving geometrical diffusion filtering, a generalization of the curvature filter (4.1) called geodesic mean curvature flow (GMCF) is useful [29]. There the diffusivity coefficient g is given by the edge detector function (3.2). In this case, a speed of evolution of contour lines depends on gradients of smoothed data. On the contrary to previous linear and nonlinear diffusion models, the surface MCF and the surface GMCF doesn't conserve the average value of data during the filtering. In the following sections, we present a numerical discretization of these models on the closed surface, and we describe their behaviour on experiments of filtering artificial data.

4.1 The surface mean curvature flow

The level set equation (4.1) is regularized by the Evans-Spruck ε-regularization [30]

$$|\nabla u| \approx |\nabla u|_\varepsilon = \sqrt{\varepsilon^2 + |\nabla u|^2}. \tag{4.2}$$

The ε-regularized Eq. (4.1) with $g = 1$ represents the regularized surface MCF model in the form

$$\partial_t u = |\nabla_s u|_\varepsilon \nabla_s \cdot \left(\frac{\nabla_s u}{|\nabla_s u|_\varepsilon} \right). \tag{4.3}$$

To get the numerical approximation of the equation (4.3), we use the same space discretization and time derivative approximation as we use in the section 2.1. After applying backward difference we get an approximation of the equation (4.3) in the form

$$\frac{1}{|\nabla_s u^{j-1}|_\varepsilon} \frac{u^j - u^{j-1}}{\tau} = \nabla_s \cdot \left(\frac{1}{|\nabla_s u^{j-1}|_\varepsilon} \nabla_s u^j \right). \tag{4.4}$$

Note that term $|\nabla_s u|_\varepsilon$ is taken from the previous time step. Then, integrating (4.4) over the finite volume V_i, applying (1.13) and taking into account geometry of the boundary ∂V_i we get the form

$$\int_{V_i} \frac{1}{|\nabla_s u^{j-1}|_\varepsilon} \frac{u^j - u^{j-1}}{\tau} dx = \sum_{q=1}^{Q_i} \int_{\partial V_{iq}} \frac{1}{|\nabla_s u^{j-1}|_\varepsilon} \nabla_s u^j \cdot \vec{\eta}_{iq} dS. \tag{4.5}$$

Subsequently, we use equations (2.4), (2.5) and (2.6) to approximate surface gradients. The regularization of the approximation of surface gradient on the triangle is denoted as $|\vec{P}_{T_{iq}}|_\varepsilon$ and defined according to (4.2) in the form

$$|\vec{P}_{T_{iq}}|_\varepsilon = \sqrt{\varepsilon^2 + |\vec{P}_{T_{iq}}|^2}. \tag{4.6}$$

Then we can approximate integral of $|\nabla_s u^{j-1}|_\varepsilon$ over the finite volume in the left-hand side as an average value of the surface gradient on the co-volume in the form

$$|\vec{P}^{j-1}_{V_{iq}}| = \frac{\sum_{q=1}^{Qi} |\vec{P}^{j-1}_{T_{iq}}|_\varepsilon [m(e^1_{iq}) + m(e^2_{iq})]}{\sum_{q=1}^{Qi} [m(e^1_{iq}) + m(e^2_{iq})]}. \tag{4.7}$$

After analogous steps as described in the section 2.1 we obtain the numerical scheme

$$\frac{m(V_i)}{|\vec{P}^{j-1}_{V_{iq}}|_\varepsilon} \frac{u_i^j - u_i^{j-1}}{\tau} = \sum_{q=1}^{Q_i} \left[m(e^1_{iq}) \vec{\eta}^1_{iq} \cdot \frac{1}{|\vec{P}^{j-1}_{T_{iq}}|_\varepsilon} \vec{P}^j_{T_{iq}} + m(e^2_{iq}) \vec{\eta}^2_{iq} \cdot \frac{1}{|\vec{P}^{j-1}_{T_{iq}}|_\varepsilon} \vec{P}^j_{T_{iq}} \right], \tag{4.8}$$

$i = 1, ..., N$, which represents a semi-implicit numerical scheme for solving mean curvature flow on the closed surface.

4.2 The surface geodesic mean curvature flow

In the case of the geodesic mean curvature flow on the closed surface, the diffusivity function g in (4.1) is given by the edge detector function (3.2). After ε-regularization the model is defined in the form

$$\partial_t u = |\nabla_s u|_\varepsilon \nabla_s \cdot \left(g(|\nabla_s u^\sigma|) \frac{\nabla_s u}{|\nabla_s u|_\varepsilon} \right). \tag{4.9}$$

To approximate (4.9) we apply the similar approach as we use in the case of the surface MCF. The final semi-implicit scheme in the form

$$\frac{m(V_i)}{|\vec{P}^{j-1}_{V_{iq}}|_\varepsilon} \frac{u_i^j - u_i^{j-1}}{\tau} = \sum_{q=1}^{Q_i} \left[m(e^1_{iq}) \vec{\eta}^1_{iq} \cdot \frac{g(|\vec{P}^{\sigma,j-1}_{T_{iq}}|)}{|\vec{P}^{j-1}_{T_{iq}}|_\varepsilon} \vec{P}^j_{T_{iq}} + m(e^2_{iq}) \vec{\eta}^2_{iq} \cdot \frac{g(|\vec{P}^{\sigma,j-1}_{T_{iq}}|)}{|\vec{P}^{j-1}_{T_{iq}}|_\varepsilon} \vec{P}^j_{T_{iq}} \right], \tag{4.10}$$

$i = 1, ..., N$, represents the approximation of the GMCF on the closed surface. The evolution of contour lines in the GMCF model is affected by the edge detector function. This extension causes a slow down of such evolution if the contour line yields high values of surface gradients. The difference between MCF and GMCF is very similar to the difference between linear model and surface Perona-Malik nonlinear model. Similarly, as in the case of surface Perona-Malik model, the edge detector is step by step evolving in time and give us an opportunity to preserve main structures in the data and effectively reduce the noise. In both model, the parameter ε, $0 < \varepsilon \leq 1$ shifts the model from the mean curvature flow of graph ($\varepsilon = 1$) to the mean curvature flow of level sets ($\varepsilon = 0$).

4.3 The behaviour of the surface MCF and the surface GMCF

In the experiment, we use the artificial data from the section 2.2, see Fig. 2.1 (left). We use the surface MCF and surface GMCF, and we compare filtered solutions with the previous solutions of each nonlinear diffusion filter. For both curvature driven filters, we use $\varepsilon = 10^{-5}$. Fig. 4.1 depicts the RMS of residuals (left) and the minimal RMS for each model (right).

From the Fig. 4.1, we can see, that using the surface MCF we get better RMS of residuals as we get using linear diffusion. However, the overall behaviour of the MCF is similar to linear diffusion. From the results it is obvious that the MCF successfully remove noise very quickly, but then the filter starts to shrink contour lines of structures. Nevertheless, using surface MCF seems to be a better choice than linear diffusion, in the case, if we do not need to preserve the mean value of data. The best solutions from all testing experiments of designed filters on the closed surface we get using surface GMCF. As the sensitivity parameter in the edge detector, we use the same value as we use in the case of Perona-Malik model ($H = 35\,000$). Fig. 4.2 (left) depicts solution of the GMCF after 46 time steps. We can see that in this case structures are successfully preserved. If we look on the differences between u^{46} (the solution with the minimal RMS of the residuals) and original piecewise constant function w, we can see that the most of noise is successfully removed. The largest differences are only along the boundaries of structures since noise located on these structures is partially preserved, see Fig. 4.2 (right). Note that differences are approximately from the range $(-0.1, 0.1)$.

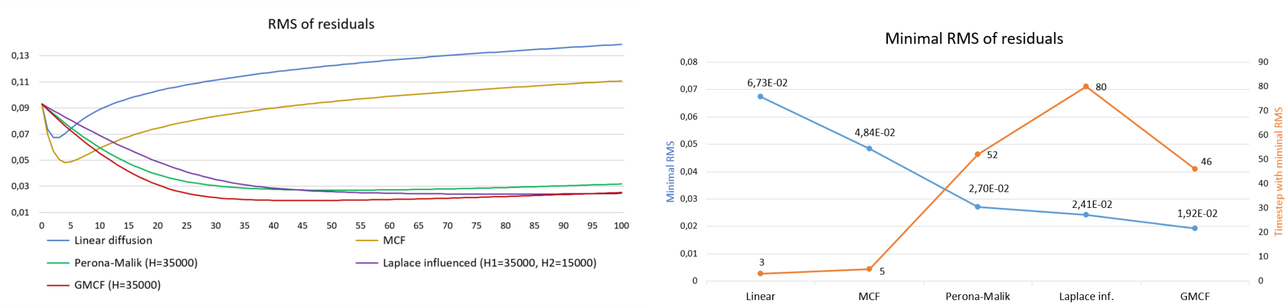

Figure 4.1: The RMS of residuals from 100 time steps left), the minimal RMS of residuals (right)

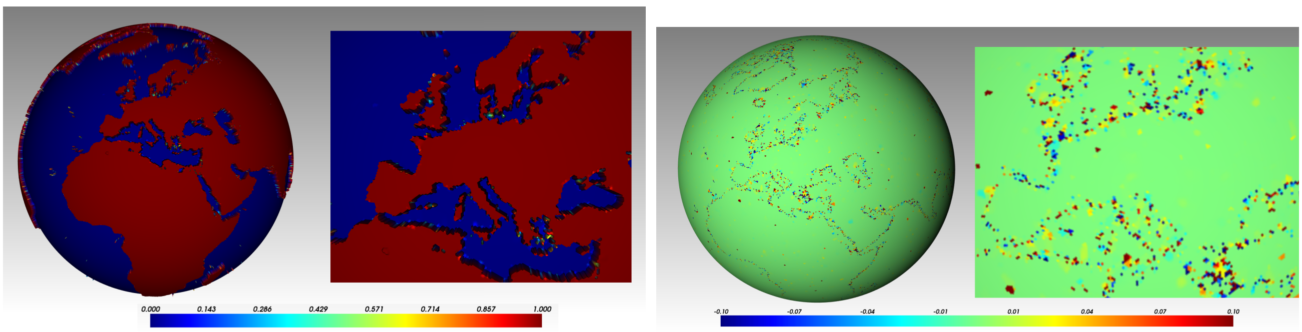

Figure 4.2: The solution of the surface GMCF after 10 timesteps (left), differences between u^{46} and w in the global and detailed area

Chapter 5

Numerical experiments on geodetic data

In this section, we present three numerical experiments where we use all developed types of diffusion filters. The first experiment aims to demonstrate filtering of noise from one component of the GOCE gravity gradients. The second experiment presents filtering of a satellite-only mean dynamic topography (MDT), where we try to reduce a typical stripping noise due to omission errors of the spherical harmonic approach. In this case, we use the modified nonlinear diffusion influenced by the surface Laplacian to pre-filter local extrema of initial data and then we use the linear diffusion and nonlinear Perona-Malik diffusion to obtain improved MDT model. The third experiment is dedicated to processing all measured components of GOCE gravity gradients using the surface MCF and surface GMCF.

5.1 Filtering of the GOCE gravity gradients in LNOF.

In this experiment, we use our developed filters to reduce the noise from measurements of the GOCE satellite mission, namely from the radial components T_{rr} of the gravity disturbing tensor available from the EGG_TRF_2 product in the local north oriented frame (LNOF). Our processed dataset represent data observed during June-July 2013. In this experiment, our computational domain represents a closed surface given by the constant altitude 245 km above a reference ellipsoid. For its discretization, we use a very refined triangulation in order to capture a dense coverage of the processed GOCE data. Namely, an octahedral grid with the resolution of 0.05 deg is constructed to generate 3D positions of 12 960 002 nodes of the regular triangulation. In these nodes, the values of the radial components T_{rr} reduced to the reference altitude are interpolated. The missing values in polar gaps (0.54% of all nodes) are generated from the GOCO03S satellite-only model up to degree 250 [31]. Such input data are then subsequently filtered by the linear and nonlinear diffusion filters. The best results we get using the nonlinear diffusion influenced by the surface Laplacian. As input parameters we use $\sigma_1 = 2\tau, \sigma_1 = \tau$, $H = 10^{12}$ and $H_2 = 10^{22}$. Fig. 5.1 (left) depicts the initial condition and the solution after 30 time steps using the nonlinear diffusion influenced by the surface Laplacian, in the detailed area and Fig. 5.1 (right) show differences between initial data and the solution.

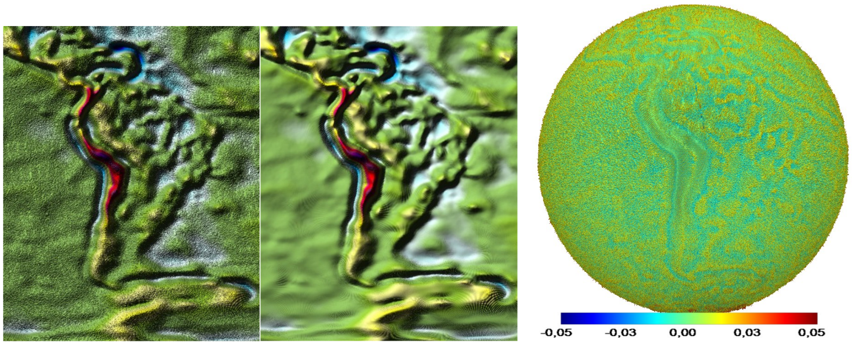

Figure 5.1: The initial condition and the solution in the detailed area (left), differences between initial data and the solution (right)

5.2 Filtering of the satellite-only MDT.

In this experiment, we present filtering of the GOCE-based satellite-only MDT. The satellite-only MDT as our initial data are given as a combination of the DTU13 mean sea surface model [32] and the geoid model evaluated from up to degree 300 [33]. Such an MDT model is significantly affected by the stripping noise due to omission errors of the spherical harmonics approach used for the geoid modelling, see Fig. 5.2 (left). Our aim is to reduce this stripping noise while to preserve important gradients that correspond to the main ocean geostrophic surface currents. In this experiment, we use the same octahedral grid with the resolution of 0.05 deg, but in this case, generated 3D positions of 12 960 002 nodes of the regular triangulation are on the surface of the reference ellipsoid.

Taking into account the nature of noise, at first, we have reduced the highest peaks of this noise. To achieve this we have used the nonlinear extrema reduction model (3.7). The detector function in the model speeds up diffusion process in nodes with the highest surface Laplacian. Those nodes represent highest values of striping noise. In the pre-filtering process we use the model parameters $\sigma = \tau = 4 \cdot 10^7$ and $H = 10^{19}$. Fig. 5.2 (right) depicts the pre-filtered data after 50 time steps. This data have been used for a final filtering. To remove the remaining noise we have used the linear diffusion and the surface Perona-Malik diffusion. In case of the linear diffusion, we use a similar time step $\tau = 4 \cdot 10^7$ as we have used in pre-filtering. This time step is also used for the nonlinear Perona-Malik diffusion. The estimated sensitivity coefficient $H = 10^{10}$ for the edge detector function is in relation to the surface gradients of processed data.

To compare the linear diffusion and the nonlinear diffusion, we have derived the ocean geostrophic surface currents, namely their zonal velocity components as well as their sea water speed. Fig. 5.3 depict sea water speed in details in regions of the main currents like the Gulf Stream, Kuroshio or Aghulas current. We can see that currents generated from data filtered by the linear diffusion represent a weaker signal, on the contrary, those generated from the nonlinear diffusion capture signal better. Stronger signal indicates that the nonlinear diffusion preserve gradient from the initial data. Consequently, the nonlinear diffusion filtering on a closed surface using the regularized surface Perona-Malik model, prefiltered by nonlinear diffusion influenced by the surface Laplacian, seems to be an efficient tool for filtering the satellite-only MDT. The pre-filtering by the modification of the nonlinear diffusion influenced by the surface Laplacian have reduced the highest values of the noise. Then the opportunity for adaptive smoothing according to the main gradients in the filtered data allows us to reduce the stripping noise efficiently while preserving important gradients that correspond to the main ocean geostrophic surface currents. Derived velocities of the ocean geostrophic surface currents have clearly shown that preserving the important gradients by the nonlinear filtering have resulted in much stronger signal than in case of the linear filtering whose uniform smoothing effect also smoothes these structures.

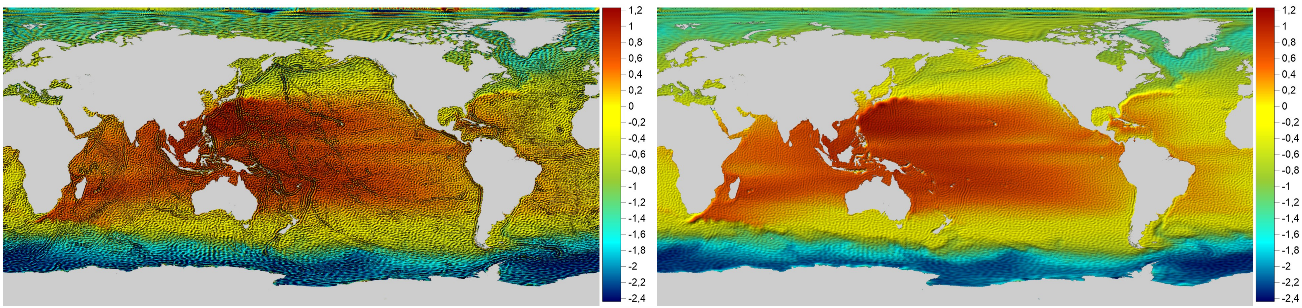

Figure 5.2: Intitial satellite-only MDT model (left), pre-filtered satellite-only MDT model (right)

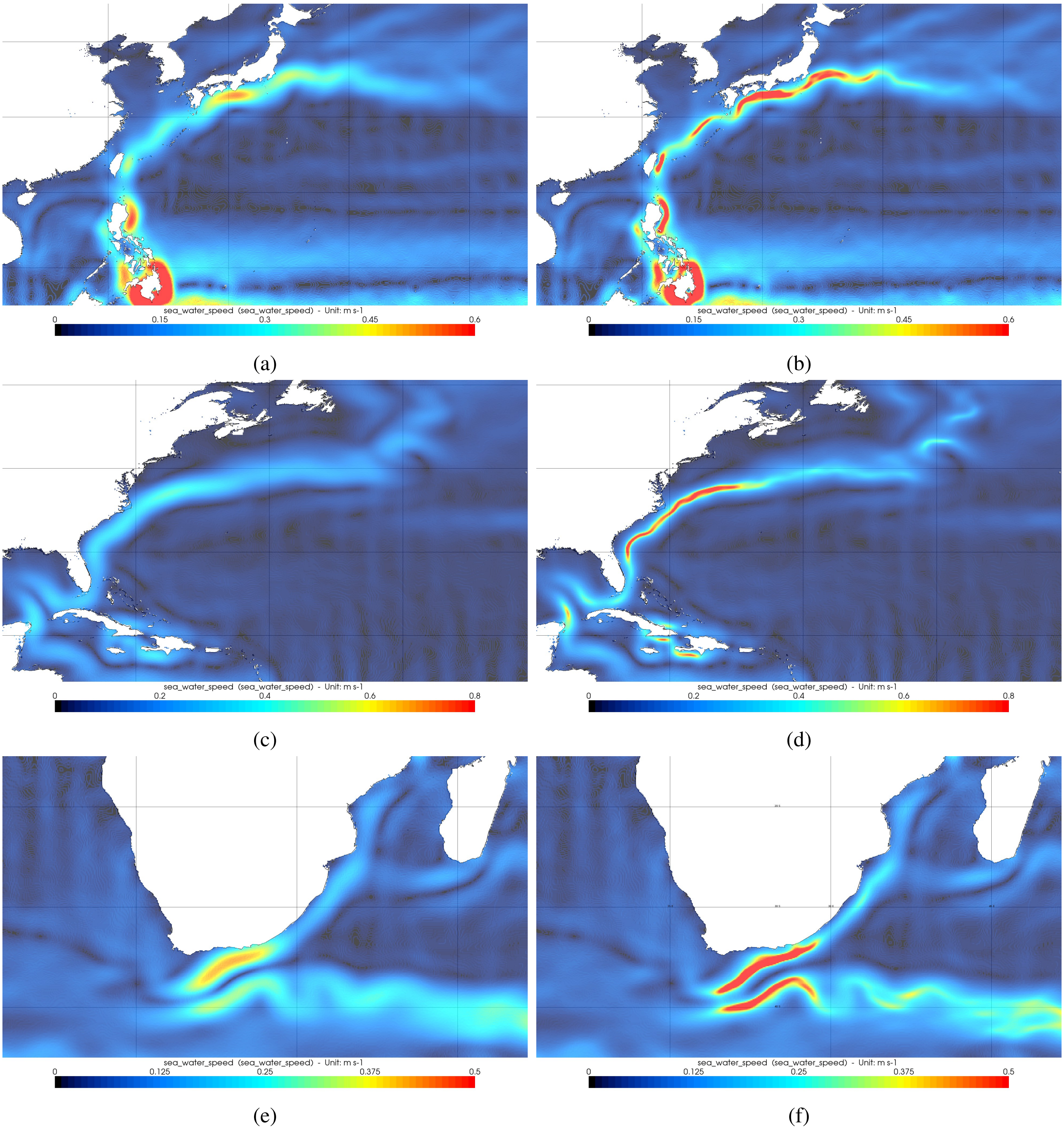

Figure 5.3: Sea water speed from filtered data obtained by the linear diffusion and filtered data obtained by the nonlinear diffusion in regions of a) b) Kuroshio, c) d) Gulf Stream, e) f) Aghulas

5.3 Filtering of the GOCE gravity gradients in GRF

In this experiment we process GOCE gravity gradients (GGs) in the gradiometer reference frame (GRF) for the period from 2013-05-28 to 2013-07-31. This data corresponds to the EGG_NOM_2 product while the GOCE GGs are corrected from the perturbations caused by the geomagnetic field [34].

In order to see better noise in the signal, we evaluate residuals between the GOCE GGs in GRF and GGs generated from the official spherical harmonics based model provided by European Space Agency (ESA), namely from the GO_CONS_GCF_2_TIM_R5 model in the LNOF transformed into the GRF. We process such residual data for ascending and descending tracks of satellite trajectory. So we consider residuals for 4 components o GOCE GGs, namely V_{xx}, V_{yy}, V_{zz} and V_{xz} for each ascending and descending track. Two others components V_{xy} and V_{yz} of GOCE GGs tensor are not considered since they are less accurately observed [35].

For a discretization of the computational domain, we use a very refined triangulation. Namely, an icosahedral grid with the resolution of 0.056 deg is constructed to generate 3D positions of 10 485 762 nodes of the regular triangulation. In these nodes, the values of each component of GOCE GGs are interpolated. The missing values in polar gaps are set to the zero. Surprisingly, the residuals include some background structures which look different for ascending and descending tracks, and have also a different location for every GGs component, see Fig. 5.4 (top-left). To overcome this problem we have decided to identify these background structure by filtering and remove them from the GOCE GGs. We use the surface MCF model for that purpose. By the MCF smaller contour lines extinct, while the smoothing of the contour lines with bigger perimeter is significantly slower. Moreover, since the MCF model does not preserve mean value, removing such data do not affect the remaining background structures. Fig. 5.4 (top-right) shows filtering by the surface MCF after 300 time steps with $\varepsilon = 10^{-5}$ for V_{xx} component of GOCE GGs both for ascending track. The filtering results represent the background structures that should be removed from the GOCE GGs. Fig. 5.4 (bottom-left) shows residuals of GOCE GGs from which we removed the background structures. It is evident that new residuals contain mainly a noise. To reduce this noise, we use the surface GMCF model. Each component is filtered by 30 time steps with parameter $H = 10^6$ and $\varepsilon = 10^{-5}$. Fig. 5.4 (bottom-right) depicts the solution of V_{xx} component on the ascending track. We can see that most of the noise is successfully removed, and the remaining filtered data will be added to spherical harmonic model and it will be used for high resolution Earth gravity field modelling in the further research steps of GOCEnumeric project.

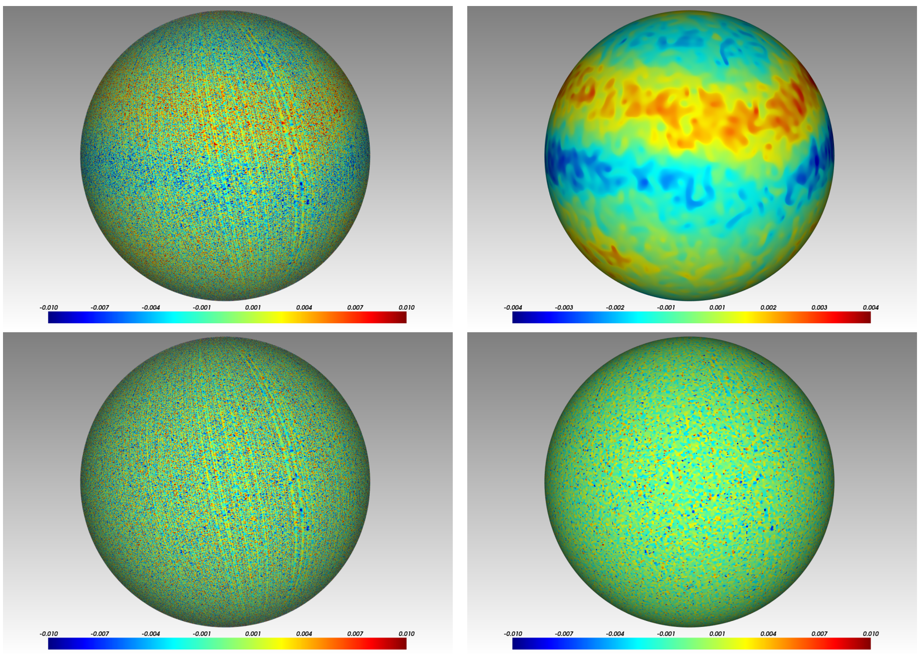

Figure 5.4: Residuals between the GOCE GGs in the GRF and GGs generated from the GO_CONS_GCF_2_TIM_R5 (top-left), filtered residuals using surface MCF (top-right), residuals with removed background structures (bottom-left), filtered residuals using surface GMCF (top-right)

References

[1] L. Alvarez, F. Guichard, P. L. Lions, and J. M. Morel, "Axioms and fundamental equations of image processing," *Archive for Rational Mechanics and Analysis*, vol. 123, no. 3, pp. 199–257, 1993.

[2] L. Alvarez and J. M. Morel, "Formalization and computational aspects of image analysis," *Acta Numerica*, vol. 3, p. 1–59, 1994.

[3] B. M. Romeny, *Geometry-Driven Diffusion in Computer Vision*. Springer, 01 1994.

[4] J. Sethian, *Level Set Methods and Fast Marching Methods: Evolving Interfaces in Computational Geometry, Fluid Mechanics, Computer Vision, and Materials Science*. Cambridge Monographs on Applied and Computational Mathematics, Cambridge University Press, 1999.

[5] J. Weickert, *Anisotropic diffusion in image processing*, vol. 1. Teubner Stuttgart, 1998.

[6] V. Caselles and J. M. Morel, "Introduction to the special issue on partial differential equations and geometry-driven diffusion in image processing and analysis," *IEEE Transactions on Image Processing*, vol. 7, pp. 269–273, March 1998.

[7] M. Nielsen, P. Johansen, O. F. Olsen, and J. e. Weickert, "Scale-space theories in computer vision," *Lecture Notes in Computer Science*, vol. 1, no. 1682, 1999.

[8] G. Sapiro, *Geometric Partial Differential Equations and Image Analysis*. Cambridge University Press, 2001.

[9] S. Osher and P. R. Fedkiw, *The Level Set Methods and Dynamic Implicit Surfaces*, vol. 57. Springer, 01 2004.

[10] J. J. Koenderink, "The structure of images," *Biological Cybernetics*, vol. 50, pp. 363–370, Aug 1984.

[11] A. Witkin, "Scale-space filtering: A new approach to multi-scale description," *Acoustics, Speech, and Signal Processing, IEEE International Conference on ICASSP'84.*, vol. 9, pp. 150–153, 1984.

[12] P.-L. Lions, "Axiomatic derivation of image processing models," *Mathematical Models and Methods in Applied Sciences*, vol. 04, pp. 467–475, 11 1994.

[13] M. Crandall, H. Ishii, P. Lions, and A. M. Society, *User's Guide to Viscosity Solutions of Second Order Partial Differential Equations*. American Mathematical Society, 1992.

[14] P. Perona and J. Malik, "Scale-space and edge detection using anisotropic diffusion," *IEEE Transactions on Pattern Analysis and Machine Intelligence*, vol. 12, pp. 629–639, Jul 1990.

[15] F. Catté, P.-L. Lions, J.-M. Morel, and T. Coll, "Image selective smoothing and edge detection by nonlinear diffusion," *SIAM Journal on Numerical Analysis*, vol. 29, no. 1, pp. 182–193, 1992.

[16] M. Nitzberg and T. Shiota, "Nonlinear image filtering with edge and corner enhancement," *IEEE Transactions on Pattern Analysis and Machine Intelligence*, vol. 14, pp. 826–833, Aug 1992.

[17] S. Kichenassamy, “The perona–malik paradox,” *SIAM Journal on Applied Mathematics*, vol. 57, no. 5, pp. 1328–1342, 1997.

[18] K. Mikula and N. Ramarosy, “Semi-implicit finite volume scheme for solving nonlinear diffusion equations in image processing,” *Numerische Mathematik*, vol. 89, pp. 561–590, Sep 2001.

[19] Z. Krivá, K. Mikula, N. Peyriéras, B. Rizzi, A. Sarti, and O. Stašová, “3d early embryogenesis image filtering by nonlinear partial differential equations,” *Medical Image Analysis*, vol. 14, no. 4, pp. 510 – 526, 2010.

[20] D. Gilbarg and N. Trudinger, *Elliptic partial differential equations of second order*. Grundlehren der mathematischen Wissenschaften, Springer, 1998.

[21] G. Dziuk and C. M. Elliott, “Finite elements on evolving surfaces,” *IMA Journal of Numerical Analysis*, vol. 27, no. 2, pp. 262–292, 2007.

[22] G. Dziuk and C. M. Elliott, “Finite element methods for surface pdes,” *Acta Numerica*, vol. 22, p. 289–396, 2013.

[23] R. Čunderlík, K. Mikula, and M. Tunega, “Nonlinear diffusion filtering of data on the earth’s surface,” *Journal of Geodesy*, vol. 87, no. 2, pp. 143–160, 2013.

[24] R. Čunderlík, M. Kollár, and K. Mikula, “Filters for geodesy data based on linear and nonlinear diffusion,” *International Journal on Geomathematics*, vol. 7, no. 2, pp. 239–274, 2016.

[25] R. Eymard, T. Gallouët, and R. Herbin, “Finite volume methods,” *Handbook of Numerical Analysis*, vol. 7, pp. 713 – 1018, 2000.

[26] D. M. Young, *Iterative Solution of Large Linear Systems*. Academic Press, 1971.

[27] H. A. van der Vorst, “Bi-cgstab: A fast and smoothly converging variant of bi-cg for the solution of nonsymmetric linear systems,” *SIAM Journal on Scientific and Statistical Computing*, vol. 13, no. 2, pp. 631–644, 1992.

[28] S. Osher and J. A. Sethian, “Fronts propagating with curvature-dependent speed: Algorithms based on hamilton-jacobi formulations,” *Journal of Computational Physics*, vol. 79, no. 1, pp. 12 – 49, 1988.

[29] V. Caselles, R. Kimmel, and G. Sapiro, “Geodesic active contours,” *International Journal of Computer Vision*, vol. 22, pp. 61–79, Feb 1997.

[30] L. C. Evans and J. Spruck, “Motion of level sets by mean curvature. i,” *J. Differential Geom.*, vol. 33, no. 3, pp. 635–681, 1991.

[31] T. Mayer-Gürr and the GOCO consortium, “The new combined satellite only model goco03s,” *Presented at the GGHS-2012 in Venice, Italy, October 9–12, 2012*, 2012.

[32] O. Andersen, P. Knudsen, and L. Stenseng, “The dtu13 mss (mean sea surface) and mdt (mean dynamic topography) from 20 years of satellite altimetry,” *International Association of Geodesy Symposia*, 01 2015.

[33] S. L. Bruinsma, C. Förste, A. O., J. C. Marty, M. H. Rio, M. S., and S. Bonvalot, “The new esa satellite only gravity field model via the direct approach,” *Geophysical Research Letters*, vol. 40, no. 14, pp. 3607–3612, 2013.

[34] C. Siemes, “Improving goce cross-track gravity gradients,” *Journal of Geodesy*, vol. 92, pp. 33–45, Jan 2018.

[35] J. Bouman, S. Fiorot, M. Fuchs, T. Gruber, E. Schrama, C. Tscherning, M. Veicherts, and P. Visser, “Goce gravitational gradients along the orbit,” *Journal of Geodesy*, vol. 85, p. 791, Oct 2011.

Zoznam publikačnej činnosti

ČUNDERLÍK, Róbert - KOLLÁR, Michal - MIKULA, Karol. Filters for geodesy data based on linear and nonlinear diffusion. In *GEM - International Journal on Geomathematics*. Vol. 7, no. 2 (2016), s. 239-274. ISSN 1869-2672. V databáze: SCOPUS ; DOI: 10.1007/s13137-016-0087-y.

KOLLÁR, Michal - MIKULA, Karol. Filtration of geodetic data on a closed surface using the new nonlinear diffusion filter. In *Advances in architectural, civil and environmental engineering [elektronický zdroj] : 25rd Annual PhD Student Conference on Architecture and Construction Engineering, Building Materials, Structural Engineering, Water and Environmental Engineering, Transportation Engineering, Surveying, Geodesy, and Applied Mathematics. Bratislava, SR, 28. 10. 2015*. 1. vyd. Bratislava : Slovenská technická univerzita v Bratislave, 2015, CD-ROM, s. 51-57. ISBN 978-80-227-4514-7.

KOLLÁR, Michal - MIKULA, Karol - ČUNDERLÍK, Róbert. Nonlinear diffusion filtering influenced by mean curvature. In *ALGORITMY 2016 : 20th Conference on Scientific Computing. Proceedings of contributed papers and posters. Podbanské, SR, 13. - 18. 3. 2016*. 1. vyd. Bratislava : Slovak University of Technology, Faculty of Civil Engineering, 2016, S. 183-193. ISBN 978-80-227-4544-4.

KOLLÁR, Michal - MIKULA, Karol - ČUNDERLÍK, Róbert. Nonlinear filtering of the satellite-only mean dynamic topography. In *Advances in Architectural, Civil and Environmental Engineering [elektronický zdroj] : 26th Annual PhD Student Conference on Architecture and Construction Engineering, Building Materials, Structural Engineering, Water and Environmental Engineering, Transportation Engineering, Surveying, Geodesy, and Applied Mathematics. 26. October 2016, Bratislava*. 1. vyd. Bratislava : Slovenská technická univerzita v Bratislave, 2016, CD-ROM, s. 44-51. ISBN 978-80-227-4645-8.

KOLLÁR, Michal - MIKULA, Karol - ČUNDERLÍK, Róbert. New software for filtering geodetic data by the nonlinear diffusion. In *Advances in Architectural, Civil and Environmental Engineering [elektronický zdroj] : 27th Annual PhD Student Conference on Applied Mathematics, Applied Mechanics, Geodesy and Cartography, Landscaping, Building Technology, Theory and Structures of Buildings, Theory and Structures of Civil Engineering Works, Theory and Environmental Technology of Buildings, Water Resources Engineering. 25. October 2017, Bratislava, Slovakia*. 1. vyd. Bratislava : Spektrum STU, 2017, CD-ROM, s. 35-41. ISBN 978-80-227-4751-6.